

Clustering promotes switching dynamics in networks of noisy neurons

Igor Franović^{1,a)} and Vladimir Klinshov^{2,b)}

¹Scientific Computing Laboratory, Center for the Study of Complex Systems, Institute of Physics Belgrade, University of Belgrade, Pregrevica 118, 11080 Belgrade, Serbia

²Institute of Applied Physics of the Russian Academy of Sciences, 46 Ulyanov Street, 603950 Nizhny Novgorod, Russia

(Received 30 November 2017; accepted 26 January 2018; published online 21 February 2018)

Macroscopic variability is an emergent property of neural networks, typically manifested in spontaneous switching between the episodes of elevated neuronal activity and the quiescent episodes. We investigate the conditions that facilitate switching dynamics, focusing on the interplay between the different sources of noise and heterogeneity of the network topology. We consider clustered networks of rate-based neurons subjected to external and intrinsic noise and derive an effective model where the network dynamics is described by a set of coupled second-order stochastic mean-field systems representing each of the clusters. The model provides an insight into the different contributions to effective macroscopic noise and qualitatively indicates the parameter domains where switching dynamics may occur. By analyzing the mean-field model in the thermodynamic limit, we demonstrate that clustering promotes multistability, which gives rise to switching dynamics in a considerably wider parameter region compared to the case of a non-clustered network with sparse random connection topology. *Published by AIP Publishing.* <https://doi.org/10.1063/1.5017822>

The striking feature of neuronal systems is that variability is reflected on two fundamentally different levels. While there is substantial knowledge on microscopic variability associated to spike trains of individual neurons, much less is known about macroscopic variability, which is a form of emergent behavior in neural networks. Macroscopic variability involves considerably longer timescales than the microscopic one, whereby its signature activity consists in slow rate oscillations, reflected in spontaneous alternation between the distinct network states. The latter are typically referred to as the UP and the DOWN states, such that in the UP state, both the firing rates and the synaptic conductances of neurons are elevated relative to the DOWN state. The switching dynamics between the collective states is especially relevant for activity of neocortical pyramidal neurons and is believed to facilitate or mediate different types of learning and memory. In this paper, we investigate the key ingredients behind switching dynamics, focusing on the interplay of different sources of noise and the network topology. In particular, we consider a clustered network of rate-based neurons and derive an effective model which describes its collective activity in terms of coupled second-order stochastic mean-field systems representing the particular clusters. The effective model is used to qualitatively analyze the mechanisms behind the switching dynamics in the non-clustered and clustered networks, comparing the associated parameter domains. For a homogeneous random network, where all neurons comprise a single cluster, switching is found only within a small parameter region in the vicinity of the pitchfork bifurcation, with the underlying mechanism resembling the motion of a noise-driven particle in a double-well potential. We demonstrate that clustering

plays a facilitatory role with respect to switching dynamics, enhancing the network multistability compared to the case of a homogeneous random network.

I. INTRODUCTION

The fascinating feature of neuronal dynamics is that variability appears in a twofold fashion. For single units, one observes the spike-train variability,¹ reflected in that the same input sequence applied to a given neuron under identical experimental conditions gives rise to different neuronal responses. Apart from the variability on the short timescale, one also encounters variability as an emergent network phenomenon²⁻⁴ associated to much longer timescales.⁵ The hallmark of macroscopic variability is irregular slow rate oscillations,^{6,7} alternatively called up-down states (UDS),⁸⁻¹⁰ which comprise large amplitude, low frequency (0.1–2 Hz) spontaneous fluctuations between the collective UP and DOWN states.¹¹ These states are characterized by clearly distinct firing rates and synaptic conductances, whereby the UP state involves neurons with depolarized membrane potential, elevated firing rates, and increased synaptic conductances relative to those in the DOWN state.¹²⁻¹⁵ Switching is induced by coherent activity of a large number of neurons and has been observed in cortical assemblies *in-vivo* during quiet wakefulness, sleep, and under the influence of anesthetic agents, as well as in certain *in-vitro* preparations.^{8,10,16-18} UDS are the prominent form of spontaneous activity of neocortical pyramidal neurons, facilitating coordination of temporal interactions between neocortex and hippocampus,^{12,19,20} which is fundamental to several types of learning and memory.^{19,21-23}

The issue of the mechanisms that give rise to macroscopic variability as an emergent network phenomenon has remained unresolved, but there are two general directions of

^{a)}Electronic mail: franovic@ipb.ac.rs

^{b)}Electronic mail: vladimir.klinshov@ipfran.ru

research.²⁴ One connects the slow rate fluctuations to deterministic networks with balanced massive excitation and inhibition,^{4,25,26} which leaves the collective dynamics highly sensitive to fluctuations. The other direction relates slow rate oscillations to bistability or multistability in attractor model networks where alternation between the coexisting states emerges due to noise,^{27,28} which acts as the finite-size effect.^{29–31} In this paper, we develop the latter framework by examining the interplay of stochastic neuronal dynamics and heterogeneous network topology on the onset and robustness of slow rate oscillations. In particular, we consider a network of rate-based neurons, focusing on how the different sources of noise, combined with the clustered network topology, give rise to slow stochastic fluctuations of the mean-rate. A qualitative insight into the mechanisms behind the slow fluctuations and the associated parameter domains is gained by developing an effective model of network activity, where the collective dynamics is described by coupled stochastic mean-field systems representing each of the clusters. The effective model for the clustered network with *random* inter- and intra-cluster connectivity is derived here for the first time, using the approach which incorporates the Gaussian closure hypothesis.^{32–34} As an intermediate result, we determine how the different sources of noise from local dynamics as well as statistical heterogeneity of the connection topology contribute to noise at the macroscopic level. This presents generalization of our previous work, where we have considered bistability and slow fluctuations in a network with simple random connection topology.^{30,35}

Investigating the impact of clustered topology on collective dynamics is biologically plausible, given that neural networks with statistically inhomogeneous wiring are inherent to mammalian neocortex,^{36,37} where the clustered structures with stronger synapses and increased connection probability make up the so-called cell assemblies. Earlier studies have indicated that clustered connectivity could give rise to bistability or multistability,^{4,25,38} potentially allowing for switching dynamics between interacting populations, considered as a likely paradigm for decision-making processes during perception or cognition. In this study, we demonstrate that clustering promotes multistability, thereby substantially enhancing the parameter domain admitting the slow rate fluctuations, as compared to a network with simple random connection topology.

The paper is organized as follows. In Sec. II, we present the key points of the derivation of the effective model for collective dynamics of the clustered network, explicitly demonstrating how the neuronal noise and network heterogeneity contribute to different finite-size effects. In Sec. III, we analyze how the network multistability and switching dynamics are influenced by the clustered topology. It is first indicated that in the absence of clustering, switching occurs in a relatively narrow parameter domain, whereby its mechanism resembles the noise-driven motion of a particle in a double-well potential. Then, we show that by introducing clustering, one enhances the network multistability, which ultimately makes the switching phenomenon considerably more robust. In Sec. IV, we provide a brief summary and discussion of the results obtained.

II. DERIVATION OF THE MEAN-FIELD MODEL

We consider a network comprising N neurons arranged into clusters, such that intra-cluster connectivity is larger than the connectivity between neurons from different clusters. The local dynamics of a given neuron i from cluster X follows the rate model^{30,35,39,40}

$$\frac{dr_{Xi}}{dt} = -\lambda_X r_{Xi} + H(v_{Xi}) + \sqrt{2D_X} \xi_{Xi}(t), \quad (1)$$

where λ_X defines the rate relaxation time, $\xi_{Xi}(t)$ denotes the intrinsic neuronal noise which typically derives from stochastic opening of ion-gating channels, whereas H is the nonlinear gain function, whose form will be specified further below. The total input to a neuron $v_{Xi} = u_{Xi} + I_X + \sqrt{2B_X} \eta_{Xi}(t)$ consists of a synaptic input $u_{Xi} = \sum_Y \kappa_{YX} \sum_j a_{YXji} r_{Yj}$ and the external bias current I_X , while fluctuations in the embedding environment are accounted for by synaptic (external) noise $\eta_{Xi}(t)$, characterized by B_X . The coupling scheme is given by the adjacency matrix $a_{YXji} \in \{0, 1\}$, with the notation a_{YXji} referring to the link which projects from neuron j in cluster Y to neuron i from cluster X . Coupling weights between two clusters or within a single cluster are assumed to be homogeneous, whereby we adopt the scaling $\kappa_{YX} = K_{YX}/N$. To improve readability, a summary of the most relevant notation is provided in Table I. Both external and intrinsic fluctuations are represented by Gaussian white noise terms which satisfy $\langle \langle \xi_{Xi}(t) \xi_{Yj}(t') \rangle \rangle = \langle \langle \eta_{Xi}(t) \eta_{Yj}(t') \rangle \rangle = \delta_{XY} \delta_{ij} \delta(t-t')$ and $\langle \langle \xi_{Xi}(t) \eta_{Yj}(t') \rangle \rangle = 0$.

The mean-field model involves a Gaussian closure hypothesis,^{32–34,41} such that the collective dynamics of each cluster X is described by the mean-rate R_X and the associated variance S_X

$$R_X = \frac{1}{N_X} \sum_i r_{Xi} \equiv \langle r_{Xi} \rangle, \\ S_X = \langle r_{Xi}^2 \rangle - R_X^2, \quad (2)$$

where $N_X = n_{xN}$ is the size of the cluster X , whereas $\langle \cdot \rangle$ refers to averaging over the neurons within the given cluster. The network behavior will be represented in terms of dynamics of interacting mean-field systems, each attributed to the

TABLE I. Summary of notation in Sec. II.

λ_X	Relaxation time of units in cluster X
D_X	Intensity of internal noise in cluster X
B_X	Intensity of external noise in cluster X
I_X	External current to cluster X
U_X	Average input to cluster X
$N_X \equiv n_{xN}$	Size of cluster X
K_{YX}	Strength of couplings projecting from cluster Y to cluster X
$\kappa_{YX} \equiv K_{YX}/N$	Normalized coupling strength
a_{YXji}	Element of adjacency matrix characterizing links projecting from neuron j of cluster Y to neuron i in cluster X
p_{YX}	Connection probability from cluster Y to cluster X
R_X	Mean rate of cluster X
S_X	Rate variance in cluster X

particular cluster. Our immediate goal is to derive a second-order stochastic mean-field (macroscopic) model for an arbitrary cluster by appropriately averaging the local (microscopic) neuronal dynamics. To this end, we first introduce an Ansatz regarding the local variables,^{30,35} which will ultimately allow us to treat the nonlinear threshold term $H(v_{Xi})$. In particular, one assumes that r_{Xi} may be written as $r_{Xi} = R_X + \sqrt{S_X} \rho_{Xi}$,⁴² where ρ_{Xi} is a set of variables that satisfies $\langle \rho_{Xi} \rangle = 0$, $\langle \rho_{Xi}^2 \rangle = 1$, as follows from definition (2). Using the Ansatz, the total input v_{Xi} to the neuron may be rewritten as $v_{Xi} = U_X + \delta v_{Xi}$, where

$$U_X = I_X + \frac{1}{N} \sum_Y K_{YX} p_{YX} N_Y R_Y, \quad (3)$$

$$\delta v_{Xi} = \frac{1}{N} \sum_Y K_{YX} R_Y \nu_{YXi} + \frac{1}{N} \sum_Y K_{YX} \sqrt{S_Y} \sigma_{YXi}. \quad (4)$$

In particular, Eq. (3) presents the assembly-averaged input to cluster X , with p_{YX} denoting the connectedness probability from cluster Y to cluster X . The deviation δv_{Xi} from the average input U_X contains two terms, namely, the ‘‘topological’’ and the ‘‘dynamical’’ one, whereby $\nu_{YXi} = \sum_j a_{YXji} - p_{YX} N_Y$ accounts for the deviation from the average number of connections $p_{YX} N_Y$, and $\sigma_{YXi} = \sum_j a_{YXji} \rho_{Yj}$ describes the effect of local rate fluctuations. Equations (3) and (4) enable one to expand $H(v_{Xi})$ about U_X , which proves crucial for deriving the reduced system for cluster dynamics. In particular, one obtains $H(v_{Xi}) = H_{0X} + H_{1X} \delta v_{Xi} + H_{2X} \delta v_{Xi}^2$, where we have introduced notation $H_{0X} \equiv H(U_X)$, $H_{1X} = \frac{dH}{dv_{Xi}}(U_X)$, $H_{2X} = \frac{d^2H}{2dv_{Xi}^2}(U_X)$. From the latter expression and the definition of R_X , one obtains

$$\begin{aligned} \frac{dR_X}{dt} = & -\lambda_X \langle r_{Xi} \rangle + H_{0X} + 2B_X H_{2X} + H_{1X} \langle \Gamma_{1X} \rangle \\ & + H_{2X} \langle \Gamma_{2X} \rangle + \sqrt{2D_X} \langle \zeta_{Xi}(t) \rangle, \end{aligned} \quad (5)$$

with $\langle \Gamma_{1X} \rangle$ and $\langle \Gamma_{2X} \rangle$ given by

$$\begin{aligned} \langle \Gamma_{1X} \rangle = & \frac{1}{N} \sum_Y K_{YX} R_Y \langle \nu_{YXi} \rangle + \frac{1}{N} \sum_Y K_{YX} \sqrt{S_Y} \langle \sigma_{YXi} \rangle \\ & + \sqrt{2B_X} \langle \eta_{Xi} \rangle, \end{aligned} \quad (6)$$

$$\begin{aligned} \langle \Gamma_{2X} \rangle = & \frac{1}{N^2} \sum_{YZ} K_{YX} K_{ZX} R_Y R_Z \langle \nu_{YXi} \nu_{ZXi} \rangle \\ & + \frac{1}{N^2} \sum_{YZ} K_{YX} K_{ZX} \sqrt{S_Y S_Z} \langle \sigma_{YXi} \sigma_{ZXi} \rangle \\ & + \frac{2}{N^2} \sum_{YZ} K_{YX} K_{ZX} R_Y \sqrt{S_Z} \langle \nu_{YXi} \sigma_{ZXi} \rangle \\ & + \frac{2\sqrt{2B_X}}{N} \sum_Y K_{YX} R_Y \langle \nu_{YXi} \eta_{Xi}(t) \rangle \\ & + \frac{2\sqrt{2B_X}}{N} \sum_Y K_{YX} \sqrt{S_Y} \langle \sigma_{YXi} \eta_{Xi}(t) \rangle. \end{aligned} \quad (7)$$

In order to calculate the final expression for the cluster mean-rate, one has to estimate the terms containing ν_{YXi} and σ_{YXi} and the associated averages. We have been able to carry this

out in a systematic fashion, assessing the order of each term. Ultimately, the stochastic mean-field model will include stochastic terms as finite-size effects, whereby we neglect the terms whose order is higher than $\mathcal{O}(1/N)$. In Subsection II A, we briefly discuss how one may determine the contributions from each term comprising $\langle \Gamma_{1X} \rangle$ and $\langle \Gamma_{2X} \rangle$.

A. Evaluating the finite-size effects

Let us first address the terms ν_{YXi} , which by definition present the deviation from the average number of links $p_{YX} N_Y$ projecting from cluster Y to a given node i of subassembly X . From the theory of complex networks, it is known that the average over the ensemble of different network configurations, which we denote by $[\cdot]$, is $[\nu_{YXi}] = 0$, whereas the associated variance is $[\nu_{YXi}^2] = p_{YX}(1 - p_{YX})N_Y$. By these arguments, it follows that $\langle \nu_{YXi} \rangle$ contributes to a constant random parameter dependent on the particular network configuration, which is manifestation of the quenched randomness introduced by fixing the given configuration. The variance of such a term between the different configurations is approximately $[\langle \nu_{YXi} \rangle^2] = \frac{p_{YX}(1-p_{YX})N_Y}{N_X} \approx \widetilde{p}_{YX} N_Y / N_X$, where $\widetilde{p}_{YX} = p_{YX}$ for the sparse connectivity $p_{YX} \ll 1$ and $\widetilde{p}_{YX} = 0$ in the limit of strong connectivity $p \sim 1$. Note that the division by N_X comes from the fact that the variance of a sum of independent random variables is equal to the sum of variances of the given variables. The terms $\langle \nu_{YXi} \nu_{ZXi} \rangle$ may be treated in a similar fashion, though one has to distinguish between the cases $Y = Z$ and $Y \neq Z$. If $Y = Z$, one may clearly use the estimate $[\langle \nu_{YXi}^2 \rangle] = p_{YX}(1 - p_{YX})N_Y \approx p_{YX} N_Y$, while if $Y \neq Z$, the terms $\langle \nu_{YXi} \nu_{ZXi} \rangle$ contribute to a random constant parameter, whose variance over the ensemble of different network configurations may be evaluated as $[\langle \nu_{YXi} \nu_{ZXi} \rangle^2] = p_{YX} N_Y p_{ZX} N_Z / N_X$.

The terms containing σ_{YXi} may heuristically be approached as follows. From the definition, it follows that $\sigma_{YXi} = \sum_j a_{YXji} \rho_{Yj} = \sum_{j \in \mathcal{C}_{YXi}} \rho_{Yj}$, i.e., the sum runs over the subassembly of neurons from cluster Y which project to neuron i from cluster X . By construction, such subassembly contains a small number of units $p_{YX} N_Y$, if the connectivity between clusters Y and X is sparse ($p_{YX} \ll 1$). In the limit of strong connectivity ($p_{YX} \sim 1$), one has the sum $\sigma_{YXi} \approx 0$, because the departure from the limit case $p_{YX} = 1$ due to the subset of neurons that do not project from Y to Xi is small. Though one cannot say *a priori* anything regarding the distribution of ρ_{Yj} , in the first approximation, one may consider them as a set of normally distributed random variables of zero mean and unit variance. This enables us to treat σ_{YXi} as a set of normally distributed random variables of zero mean and variance $p_{YX} N_Y$. Also note that the correlation $\sigma_{YXk} \sigma_{YXi} = \sum_{i,j} a_{YXik} a_{YXjl} = p_{YX}^2 N_Y$, which is small due to smallness of p_{YX} , such that all the terms σ_{YXi} may be taken as uncorrelated.

The above arguments imply that $\langle \sigma_{YXi} \rangle$ may be evaluated as effective noisy terms of zero mean and variance $[\langle \sigma_{YXi} \rangle^2] = (1 - \widetilde{p}_{YX}) N_Y / N_X$. By the above line of arguments, it may explicitly be shown that the variables σ_{YXi}^2 can effectively be

treated as random variables whose mean and variance satisfy $[\sigma_{YXi}^2] = p_{YX}N_Y$ and $[\sigma_{YXi}^4] - [\sigma_{YXi}^2]^2 = 2p_{YX}^2N_Y^2$, respectively.

B. Equations of the mean-field model

The results from Subsection II A enable us to systematically evaluate the contributions from all the terms on the r.h.s. of (6) and (7). Focussing on (6) first, one finds that the three associated terms give rise to finite-size effects of different nature. In particular, the first term contains an effective random parameter associated to the given network configuration and may be written as $\frac{1}{N}K_{YX}R_Y\sqrt{p_{YX}N_Y/N_X}\gamma_1$, where γ_1 is a $\mathcal{N}(0, 1)$ variable. The latter should not be confound with noise, as γ_1 can be treated as a random parameter. The second element from the r.h.s. of (6) contributes to pseudo-noise of the order $\mathcal{O}(1/N)$, which is given by $\frac{1}{N}K_{YX}\sqrt{S_Y}\sqrt{p_{YX}N_Y/N_X}\gamma_2(t)$. One refers to it as pseudo-noise because it fluctuates randomly in time, but does not derive from the actual microscopic noise. The third term on the r.h.s. of (6) presents the sum of local external noises, which gives rise to a genuine macroscopic noise $\sqrt{2B_X/N_X}\zeta_X(t)$.

As far as $\langle \Gamma_{2X} \rangle$ is concerned, the terms containing $\langle \nu_{YXi}\nu_{ZXi} \rangle$ and $\langle \sigma_{YXi}\sigma_{ZXi} \rangle$ for $Y=Z$ together provide the $\mathcal{O}(1/N)$ deterministic finite-size effect of the form $\frac{1}{N}K_{YX}^2p_{YX}n_Y(R_Y^2 + S_Y)$. The remaining contribution from such terms for $Y=Z$ and $Y \neq Z$ amounts to random constant parameters and pseudo-noises, respectively, whose intensity is of the order $\mathcal{O}(N^{-3/2})$ and as such can be neglected. As an illustration, we state that the terms involving $\langle \nu_{YXi}\nu_{ZXi} \rangle$ for $Y \neq Z$ may be evaluated as $\frac{1}{N^2}K_{YX}K_{ZX}R_YR_Z\sqrt{p_{YX}p_{ZX}N_YN_Z/N_X}$, which is indeed $\mathcal{O}(N^{-3/2})$. Finally, averaging over all the terms at the r.h.s. of (7) containing the genuine noises $\eta_{Xi}(t)$ at the macroscopic level provides stochastic effects of the order $\mathcal{O}(1/N^2)$, which can also be neglected within our mean-field model.

Collecting all the results stated so far, one arrives at the following equation for the dynamics of the cluster mean-rate:

$$\begin{aligned} \frac{dR_X}{dt} = & -\lambda_X R_X + H_{0X} + 2B_X H_{2X} \\ & + H_{2X} \sum_Y K_{YX}^2 p_{YX} n_Y (R_Y^2 + S_Y) / N \\ & + \sqrt{\Psi_X} \beta(t) + \sqrt{\Omega_X} \eta, \end{aligned} \quad (8)$$

where the ‘‘macroscopic’’ noise is of intensity $\Psi_X = \frac{1}{N}(2D_X + 2B_X H_{1X}^2) + \frac{1}{N} H_{1X}^2 \sum_Y K_{YX}^2 p_{YX} \frac{N_Y}{N_X} S_Y$, and the associated random variable $\beta(t)$ is Gaussian distributed. The macroscopic noise is made up of three terms which may be interpreted as follows. The two terms in the first bracket represent the contribution from the local intrinsic and external noise translated to macroscopic level, whereby the latter is manifested as multiplicative, rather than the additive noise. The third term is of different character and essentially reflects the impact of local fluctuations in the input provided to each neuron within the cluster. Apart from this, Eq. (8) also contains a random term where η is just a constant random number $\mathcal{N}(0, 1)$, whereas the associated intensity is $\Omega_X = \frac{1}{N} H_{1X}^2 \sum_Y K_{YX}^2 p_{YX} \frac{N_Y}{N_X} R_Y^2$. Note that the latter factor derives

from the topological ‘‘uncertainty’’ effect related to quenched randomness, in a sense that each particular network realization is characterized by distinct deviations from the average connectivity degree.

Starting from the definition and applying the Itô derivative, one may use analogous methods to obtain the final equation for the variance S_X . We omit the details of the lengthy calculation, but just state that here we also neglect the deterministic finite-size correction of the order of $\mathcal{O}(1/N)$, as well as all the noisy terms and the terms related to uncertainty parameter derived from the particular network realization. The final equation for the variance then becomes

$$\frac{dS_X}{dt} = -2\lambda_X S_X + 2B_X H_{1X}^2 + 2D_X. \quad (9)$$

Equations (8) and (9) make up the second-order stochastic mean-field model describing the collective activity of each cluster within the network. To complete the model, it is necessary to specify the gain function H . In general, the gain function should meet the requirements that it is zero for sufficiently small input and that it saturates for large enough input, whereas for intermediate input values, H should just be smooth and monotonous. For convenience of analytical study,^{30,35} we adopt the following form of H :

$$H(Q) = \begin{cases} 0, & Q \leq 0, \\ 3Q^2 - 2Q^3, & 0 < Q < 1, \\ 1, & Q \geq 1. \end{cases} \quad (10)$$

III. ANALYSIS OF THE MEAN-FIELD MODEL AND SWITCHING DYNAMICS

In order to demonstrate the facilitatory role of clustering on switching dynamics more explicitly, we first investigate how the switching emerges in case of statistically homogeneous random network and then draw comparison to scenario the involving clustered network topology. In both instances, the analysis of the mean-field model in the thermodynamic limit $N \rightarrow \infty$ is used to gain qualitative insight into the parameter domains supporting coexistence of different stationary states. The latter is a necessary ingredient for the onset of slow rate fluctuations, which emerge due to the finite-size effect. It will be demonstrated that the switching dynamics in clustered and non-clustered networks are based on different mechanisms, which we relate to the finding that clustering promotes network multistability.

A. Slow rate fluctuations in a non-clustered network

Let us first consider the deterministic dynamics of the non-clustered network with uniform coupling strengths. Given that this case has been analyzed in detail in our previous papers,^{30,35} here we provide only a brief summary of the main results.

The network behavior is described by the deterministic part of the system Eqs. (8) and (9), whereby (4) implies that the average input to each neuron amounts to $U = I + KpR = I + \alpha R$, with $\alpha = Kp$ being the connectivity parameter. Note that S generally affects the R dynamics only via $\mathcal{O}(1/N)$

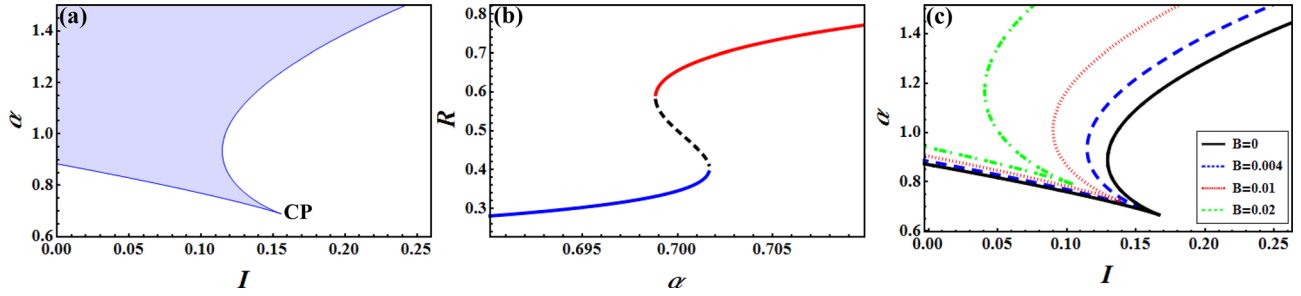


FIG. 1. Analysis of the mean-field model of a non-clustered random network in the thermodynamic limit $N \rightarrow \infty$. (a) Bistability domain (highlighted region) in the $(I - \alpha)$ plane is bounded by two branches of saddle-node bifurcations. The latter meets at the cusp point CP, located at (I_p, α_p) , where the pitchfork bifurcation occurs. External noise is set to $B = 0.004$, whereas $D = 0.02$. (b) $R(\alpha)$ dependence within the bistability tongue ($I = 0.15, B = 0.004$) shows coexistence between the UP and the DOWN state. (c) Shift of bistability domain for increasing $B \in \{0, 0.004, 0.01, 0.02\}$.

terms, which contribute to the small deterministic correction term and the macroscopic noise. Thus, in the thermodynamic limit, one may neglect the S evolution and replace it with the corresponding stationary value $S_0 = (B_\chi H_1^2 + D)/\lambda$. For simplicity, we adopt $\lambda = 1$ in the remainder of the paper. In order to analyze the stability of (8) in the limit $N \rightarrow \infty$, it is convenient to rewrite it in terms of the average input U as^{30,35}

$$\frac{dU}{dt} = -2\alpha U^3 + 3\alpha U^2 - 12\alpha B U - U + 6\alpha B + I. \quad (11)$$

Equation (11) always admits at least one stable stationary state. For the given external noise B , the onset of bistable regime is associated to the pitchfork bifurcation that occurs at $\alpha_p = 2/(3(1 - 8B))$ and $I_p = (1 - \alpha_p)/2$. From this cusp point emanate two branches of saddle-node bifurcations, which outline the bistability “tongue” where the UP and the DOWN states characterized by the high and low mean-rates coexist, cf. Fig. 1(a). In particular, the upper curve corresponds to creation of the UP state, whereas the lower curve coincides with annihilation of the DOWN state. Within the coexistence region, the two stable states are separated by the unstable state, cf. Fig. 1(b), whereby the level of the unstable state decreases with α . This confines the attraction basin of the DOWN state, facilitating the prevalence of the UP state at higher connectivity. Figure 1(c) further shows that for increasing B , the bistability domain gets shifted toward larger α . Note that the change of α is achieved by increasing the coupling strength K while the connectedness probability $p = 0.2$ is kept fixed to conform to the case of sparse random network, which maintains certain biological plausibility.

The mechanism behind switching dynamics in the non-clustered network may be explained by analyzing the finite-size effect and is reminiscent of the noise-driven motion of a

particle in a double-well potential. The analogy lies in the fact that the macroscopic noise, as the finite-size effect, allows for the network mean-rate to jump between the minima of the potential, which correspond to the two stationary levels of the deterministic part of the mean-field model, see the example of $R(t)$ series in Fig. 2(a). Replacing S by its stationary value, Eq. (8) for the stochastic dynamics of the mean-rate may be written in term of U as

$$\frac{dU}{dt} = -\frac{dV}{dU} + \sqrt{\Psi}\xi, \quad (12)$$

where V presents the potential $V(U) = \alpha U^4/2 - \alpha U^3 + (6\alpha B + 1/2)U^2 - (6\alpha B + I)U + \mathcal{O}(1/N)$, whereas the macroscopic noise amounts to $\Psi = \alpha^2(2 + \alpha^2)[36BU^2(1 - U)^2 + D]/N$. In the vicinity of the pitchfork bifurcation, V indeed has the shape of a double-well potential, as illustrated in Fig. 2(b).

The described switching mechanism is generic, in a sense that one expects to observe it close to bifurcation inducing the bistability, but is not robust, given that the physically meaningful switching rates are obtained in the sufficiently small parameter domain about the bifurcation value. Beyond this area, the potential barrier becomes too high for the noise to overcome it, making the switching events extremely unlikely.

In principle, the macroscopic noise $\Psi(U)$ is multiplicative, which makes finding the analytical expression for the underlying transition rates extremely difficult. Nevertheless, in a first approximation, the setup may be reduced to the classical Kramers problem⁴³ if Ψ is replaced by its mean Ψ_m obtained by averaging over the U values between the two potential wells. Figure 3(a) illustrates that Ψ_m may be considered representative for the whole range of $\Psi(U)$ values,³⁰ especially given that the macroscopic noise is well bounded

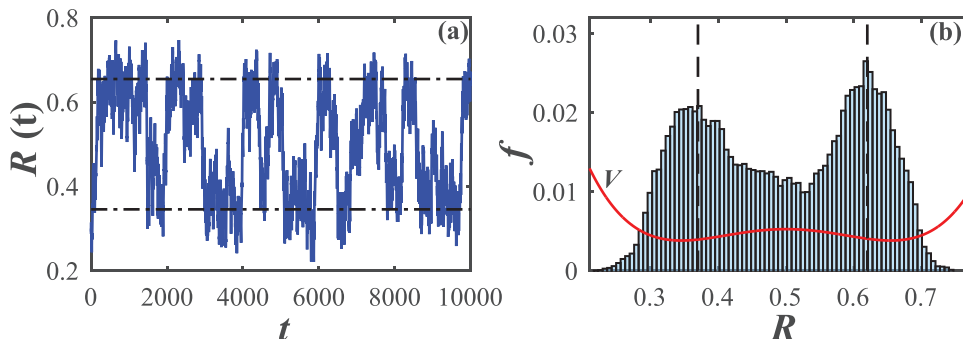


FIG. 2. Slow rate fluctuations illustrated by the $R(t)$ series in (a) and the associated stationary probability distribution $f(R)$ in (b). The results are obtained numerically for $I = 0.15, \alpha = 0.7, B = 0.004, D = 0.02$ and the network size $N = 400$. The dashed-dotted lines in (a) indicate the UP and DOWN levels of the corresponding mean-field model in the thermodynamic limit. The solid line in (b) presents the double-well potential V , cf. Eq. (12).

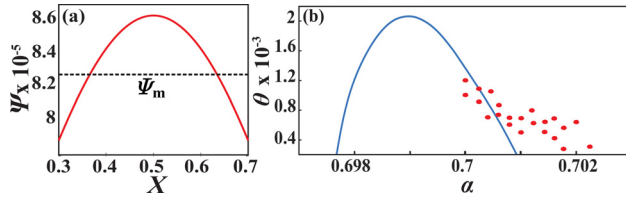


FIG. 3. (a) Macroscopic noise Ψ as a function of the mean-input X . The dotted line indicates the average Ψ_m over the relevant X range. (b) The solid line shows $\theta(\alpha)$ dependence obtained for the mean-field model via the Kramers formula (13). Dots denote the switching rates obtained numerically for $I = 0.15$, $B = 0.004$, $D = 0.02$, and $N = 400$.

within the relevant U interval. Within this framework, the first passage time between the two wells can be determined via the Kramers formula^{44–46}

$$T_{U_{\pm} \rightarrow U_{\mp}} \approx \frac{\pi}{\sqrt{|V''(U_{max})| |V''(U_{\pm})|}} \exp \left[\frac{V(U_{max}) - V(U_{\pm})}{\Psi_m} \right], \quad (13)$$

where U_{\pm} refer to the two minima of the double-well potential, whereas U_{max} denotes the location of its maximum. The total transition rate is then given by $\theta = 1/(T_{U_{+} \rightarrow U_{-}} + T_{U_{-} \rightarrow U_{+}})$. For α values in vicinity of the pitchfork bifurcation, the last expression may be used to compare with the numerical findings, cf. Fig. 3(b). One finds qualitative matching of the prediction derived from the mean-field model and the simulation within two aspects: (i) the region where $\theta(\alpha)$ is positive corresponds well to the region where the exact system exhibits slow rate fluctuations, and (ii) the order of the predicted θ values is the same as the one obtained from simulations.

B. Switching dynamics in clustered networks

In Subsection III A, we have shown that switching in homogeneous random networks is confined to the parameter domain in close vicinity of the pitchfork bifurcation. The main goal here is to demonstrate that switching in clustered networks is based on the paradigm that clustering promotes networks multistability. The outcome is that the switching phenomenon gains on robustness, in a sense that it can be found for parameter regions where it cannot be observed in statistically homogeneous random networks.

We shall show that sufficiently strong clustering supports multistability by giving rise to network states which do not exist in the non-clustered case. The increased number of network levels derives from the states with broken symmetry, where *subsets of clusters* occupy different levels, lying either in the UP or the DOWN state. By analyzing the mean-field model in the thermodynamic limit, we find that such multistability can be achieved only by varying the connectivity features of the network (topological heterogeneity), rather than by introducing the parameter heterogeneity over the subsets of network clusters. With increased multistability, the stochastic terms contributing to finite-size effect may cause the network to cross to another level just by inducing the switching event within a single cluster. The slow rate oscillations are then naturally supported by the fact that the

impact of the finite-size effect is more pronounced for individual clusters than for the entire network.

Though the system Eqs. (8) and (9) are quite general in a sense that they may be applied to a network comprising an arbitrary number of clusters of arbitrary sizes, for simplicity, we address here the case where the network consists of m equal clusters of size $N_c = N/m$. Clustering algorithm consists in rearranging the links from the homogeneous random network, such that the average connectedness probability $p = 0.2$ is preserved. We introduce additional clustering parameter g to characterize topological heterogeneity, cf. Table II for the summary of notation relevant for Sec. III B. Parameter g presents the ratio between the intra-cluster and cross-cluster connectivity, α_{in} and α_{out} , respectively, such that $\alpha_{in} = g\alpha_{out}$ with $g > 1$. Larger g implies stronger clustering, whereby the limiting case $g = 1$ describes the non-clustered network, whereas the case $g \rightarrow \infty$ corresponds to the network of disconnected clusters. One may show that α_{in} and α_{out} can be expressed in terms of the connectivity of the original homogeneous network α as

$$\alpha_{in} = \frac{gm}{m-1+g}\alpha, \quad \alpha_{out} = \frac{m}{m-1+g}\alpha. \quad (14)$$

This allows us to compare the relevant parameter domains between the homogeneous and the clustered networks.

Let us now focus on the scenario where l clusters occupy state R_a , and $m-l$ clusters lie at R_b . While the homogeneous state has the permutation symmetry Σ_m with respect to exchange of all the cluster indices, the solutions we consider now have a reduced symmetry $\Sigma_l \otimes \Sigma_{m-l}$. One may analyze the stability and bifurcations of the corresponding mean-field model in the thermodynamic limit $N \rightarrow \infty$, cf. (11). The model is given by

$$\begin{aligned} \frac{dR_a}{dt} &= -2U_a^3(R_a, R_b) + 3U_a^2(R_a, R_b) \\ &\quad + 6B(1 - 2U_a(R_a, R_b)) - R_a \\ \frac{dR_b}{dt} &= -2U_b^3(R_a, R_b) + 3U_b^2(R_a, R_b) \\ &\quad + 6B(1 - 2U_b(R_a, R_b)) - R_b, \end{aligned} \quad (15)$$

where the average input to the two groups of clusters reads

$$\begin{aligned} U_a(R_a, R_b) &= I + \frac{\alpha}{m-1+g} [(g+l-1)R_a + (m-l)R_b], \\ U_b(R_a, R_b) &= I + \frac{\alpha}{m-1+g} [lR_a + (g+m-l-1)R_b]. \end{aligned} \quad (16)$$

As for the non-clustered network, the variances S_a and S_b can be substituted by their respective stationary values

TABLE II. Summary of notation in Sec. III B.

$\alpha \equiv Kp$	Connectivity parameter of the homogeneous network
m	Total number of clusters
α_{in}	Intra-cluster connectivity
α_{out}	Inter-cluster connectivity
$g \equiv \alpha_{in}/\alpha_{out}$	Clustering parameter
$\delta \equiv 1/(g-1)$	Inverse clustering parameter

$S_i^* = (B_x H_i^2 + D)/\lambda$, with $i \in \{a, b\}$. Using (16), one may express R_a and R_b in terms of U_a and U_b via

$$\begin{aligned} R_a &= \frac{U_a - I}{\alpha} + \frac{m - l}{\alpha(g - 1)}(U_a - U_b), \\ R_b &= \frac{U_b - I}{\alpha} + \frac{l}{\alpha(g - 1)}(U_b - U_a). \end{aligned} \quad (17)$$

Inserting the latter expressions into (15), we obtain that the steady states of the mean-field model satisfy

$$\begin{aligned} I - f(U_a) + \delta(m - l)(U_b - U_a) &= 0, \\ I - f(U_b) + \delta l(U_b - U_a) &= 0. \end{aligned} \quad (18)$$

In (18), $f(U_i)$ is given by $f(U_i) = 2\alpha U_i^3 - 3\alpha U_i^2 + (1 + 12B\alpha)U_i - 6B\alpha$, which implies that the terms $I - f(U_i)$ have exactly the same form as the r.h.s. of (11) for the homogeneous random network. For convenience, we have introduced the inverse clustering parameter $\delta = (g - 1)^{-1}$, whereby the limit $\delta \rightarrow \infty$ corresponds to the non-clustered network, while the case $\delta \rightarrow 0$ coincides with ultimate clustering, i.e., the scenario where the network comprised effectively independent clusters. The system (18) naturally possesses the symmetry with respect to exchanging l and $m - l$ together with U_a and U_b ($l \leftrightarrow m - l, U_a \leftrightarrow U_b$).

Our interest lies with the inhomogeneous states where the respective stationary levels of the two groups of clusters are different, $R_a^* \neq R_b^*$. The analysis of (18) reveals that apart from the homogeneous states described in Sec. III A, one may indeed find one or two coexisting inhomogeneous states depending on the inverse clustering parameter δ under fixed (m, l, I, B) . While the system (15) and the subsequent Eqs. (16)–(18) can describe a network of arbitrary number of equal clusters, the analysis below is focused on the network of $m = 5$ clusters. This is chosen as a minimal paradigmatic example, convenient since due to symmetry, the cases $l = 1$ and $l = 2$ exhaust all the possible inhomogeneous solutions.

Onset of inhomogeneous states is investigated in detail by constructing the $\delta - I$ bifurcation diagrams (see Fig. 4). The left and the right plots refer to cases $l = 1$ and $l = 2$, respectively, with the remaining network parameters fixed to $\alpha = 0.8, B = 0.004$. For δ values less than the level indicated by the red dotted line in Fig. 4(b), there exists an I interval where two inhomogeneous solutions can coexist, whereas above the given δ , one can find only monostable inhomogeneous states.

Note that the region of coexistence between the two inhomogeneous states admits a total of 9 solutions of the mean-field model (15), cf. the notation in Fig. 4(b), whereas in the two domains with a single genuine clustered regime, one finds a total of 7 solutions of the mean-field model. Most of the curves indicated in Fig. 4 correspond to saddle-node bifurcations. In particular, the transitions from regions with 1 to regions with 3 solutions and *vice versa* coincide with creation or annihilation of the homogeneous states already described in Sec. III A. Also, the boundary between regions with 5 and 7 solutions is given by the branches of saddle-node bifurcations which meet at the cusp point where the pitchfork bifurcation occurs. Exceptions to this paradigm are the transitions involving regions with 3 and 5 solutions of the mean-field model. The latter present fold bifurcations of the inhomogeneous states within the symmetry subgroup $\Sigma_l \otimes \Sigma_{m-l}$, whereby the emanating branches correspond to an unstable fixed point and a saddle point.

A more detailed picture of the inhomogeneous states and their stability domains relative to homogeneous states may be obtained by analyzing the corresponding $R(I)$ bifurcation diagrams for fixed $(m, l, B, \delta, \alpha)$. The plots in Fig. 5 are provided for (δ, I) values supporting the coexistence of two inhomogeneous states. The top and the bottom panels refer to cases $l = 1$ and $l = 2$, respectively. In each panel, the left and the middle plots indicate the states occupied by the groups of l and $m - l$ clusters, respectively, whereas the right plot concerns the entire network (left and middle plots superimposed).

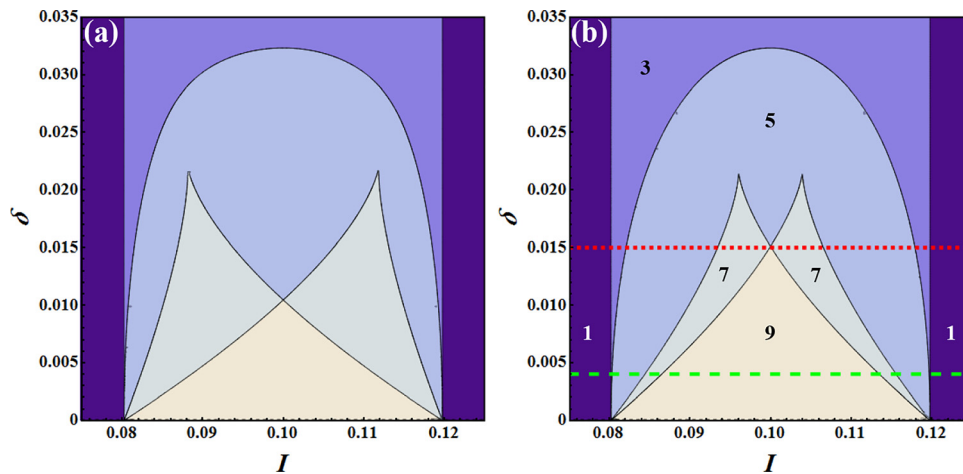


FIG. 4. Bifurcation diagrams $\delta(I)$ for the inhomogeneous solutions of the mean-field model (15). (a) corresponds to case $l = 1$, whereas (b) refers to case $l = 2$. In (b), the total number of solutions obtained for the mean-field model within the different parameter domains is indicated. The regions with 1 and 3 solutions admit only homogeneous states, while the region with 5 solutions contains unstable inhomogeneous states. The regions with 7 and 9 solutions facilitate monostable inhomogeneous states and coexistence between the two inhomogeneous states, respectively. The bistability between inhomogeneous states arises only for sufficiently strong clustering below the red dotted line, cf. the bifurcation diagrams in Fig. 5 and Fig. 6 obtained for the δ level just above the red line and the δ value indicated by the green dashed line, respectively. The remaining network parameters are $m = 5, B = 0.004, \alpha = 0.8$.

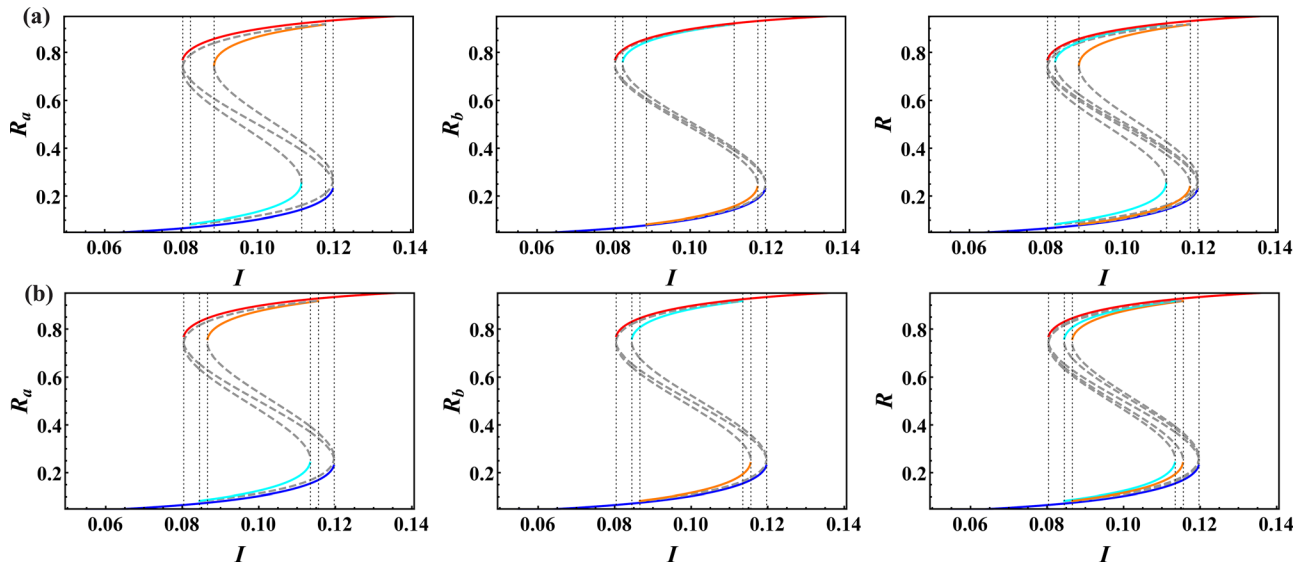


FIG. 5. Bifurcation diagrams $R(I)$ for strong clustering $\delta = 0.004$, cf. the level denoted by the green dashed line in Fig. 4(b). Panels (a) and (b) correspond to cases $l=1$ and $l=2$, respectively. The left and middle columns refer to states of particular groups of clusters R_a and R_b . The latter are superimposed in the right column to indicate the possible network states. The stable solutions are given by the solid lines, and the unstable branches are shown by the gray dashed lines. The R_a and R_b states corresponding to the same solution are presented by the same color. The remaining system parameters are $m = 5$, $B = 0.004$, $\alpha = 0.8$.

One clearly distinguishes between the regions where only one inhomogeneous solution is stable (either l clusters in the DOWN state and $m - l$ in the UP state or *vice versa*) and the central I region where two inhomogeneous solutions coexist. For instance, in the bottom panel, coexistence of two inhomogeneous states is found for $I \in (0.0866, 0.1135)$, whereas the regions with l clusters UP or DOWN as the only inhomogeneous solutions are given by $I \in (0.0845, 0.0866)$ and $I \in (0.1135, 0.1156)$. The presentation scheme is such that the solid (dashed) lines indicate the stable (unstable) branches of solutions. Note that the top-most (red solid line) and the bottom-most curves (blue solid line) in both panels

indicate the homogeneous states. In case of inhomogeneous states, the color coding is such that R_a and R_b corresponding to the same solution are assigned with the same color. As expected, the stability domains of the inhomogeneous states are smaller than the regions supporting the homogeneous states.

In Fig. 6, the $R(I)$ bifurcation diagrams for lower clustering (larger δ) are shown, which no longer admits bistability between the inhomogeneous states. The top and the bottom panels again refer to cases $l=1$ and $l=2$, respectively. From both panels, one learns that the two I intervals, where single inhomogeneous solutions exist, are separated by the I interval

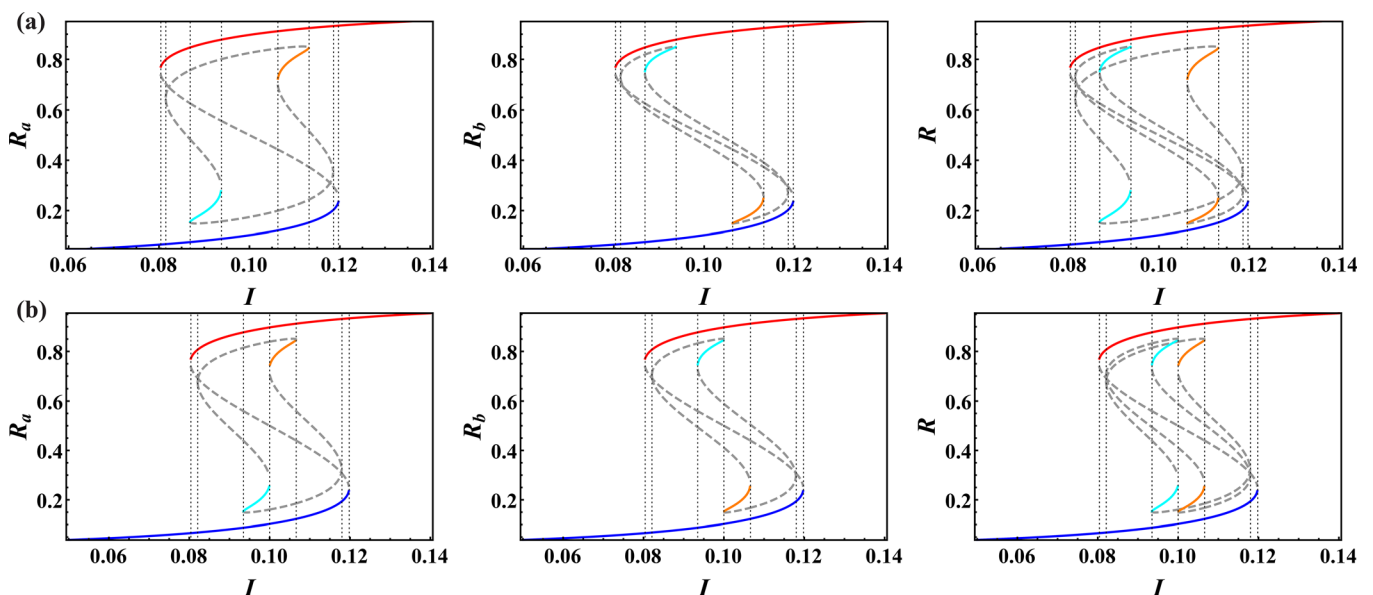


FIG. 6. Bifurcation diagrams $R(I)$ in case of weak clustering $\delta = 0.0151$, the value just above the level indicated by the red dotted line in Fig. 4(b). The top and bottom panels correspond to cases $l=1$ and $l=2$, respectively. The presentation style is the same as in Fig. 5. The remaining network parameters are $m = 5$, $B = 0.004$, $\alpha = 0.8$.

where only the two homogeneous states are available. A more detailed view of the basins of attraction of the particular states can be obtained by examining the vector fields for the relevant I values, cf. Fig. 7.

To gain a more general understanding of the multistability of the mean-field model (15), one should note that it is affected by two types of parameters, namely (i) the ones associated to homogeneous network and (ii) those characterizing the clustering. System (18) implies that the case of ultimate clustering ($\delta = 0$) leads to the same type of dynamics as that of a homogeneous network. Consequently, the area of bistability of the homogeneous network corresponds to the maximal multistability of the clustered network: each cluster may either be in the UP or the DOWN state, which yields $m + 1$ different stable solutions in total. Bistability of the homogeneous network has been addressed in Fig. 1 and has been examined in greater detail in our earlier papers.^{30,35}

The main novelty here concerns the impact of the clustering degree and its interplay with α, B , and m . As already indicated in Fig. 4, reduction of the clustering degree, i.e., increase of δ , leads to gradual extinction of the inhomogeneous states via saddle-node bifurcations. Nevertheless, we have established that the stronger average network connectivity α allows for the inhomogeneous states to occur at lower clustering, as corroborated by the shift of the relevant δ region to higher values when α is increased under all the other parameters fixed (not shown). Also, one finds that the δ region admitting inhomogeneous states reduces under increasing noise B .

In order to investigate the effect of the number of clusters m , one may introduce the ratio $\mu = l/m$ and rewrite Eq. (18) as

$$\begin{aligned} I - f(U_a) + \delta m(1 - \mu)(U_b - U_a) &= 0, \\ I - f(U_b) + \delta m\mu(U_b - U_a) &= 0. \end{aligned} \quad (19)$$

It follows that for the given ration μ , the bifurcations in the system depend only on the product $m\delta$. The latter implies that the increase in the number of clusters m leads to the onset of the relevant bifurcations for smaller δ . In other words, the more clusters present in the network, the stronger clustering is required to support the same level of multistability.

The analysis on multistability of the clustered network derived from the mean-field model is qualitative in character, but allows one to classify all the network states and gain understanding of the mechanism behind the switching dynamics.

The qualitative character of the predictions is reflected in that the mean-field model becomes the least accurate in vicinity of bifurcations where fluctuations are most pronounced, such that the finite-size effect prevails. Nevertheless, via the mean-field approach, one is also able to compare the effect of certain system parameters on the dynamics of the homogeneous and the clustered network. In particular, we are interested in comparison with respect to parameters I and α . For the homogeneous network, one finds the bistability tongue, whereby the switching dynamics occurs in close vicinity of the cusp. Using the model (15), we have constructed analogous $\delta - I$ bifurcation diagrams for the clustered network with fixed α . Our goal is to apply these results to explicitly demonstrate that multistability promoted by the clustered topology plays the facilitatory role with respect to switching dynamics. This is easily understood intuitively, as additional multistability induced by clustering implies more network levels distributed less widely. Then, switching between different levels becomes more efficient because it may be achieved just by alternations within individual clusters, and the finite-size effect within the clusters is more pronounced given their smaller size compared to the whole network.

To illustrate the impact of clustering on the onset of slow rate oscillations, we consider an example where the system parameters B, I, α are fixed to $B = 0.01, I = 0.0513, \alpha = 0.9$, respectively. For the given B , the selected (α, I) values lie deep within the bistability tongue of the homogeneous random network, viz., far from the cusp point, cf. Figure 1(c). The corresponding time series of the network mean-rate $R_N(t)$ and the associated stationary probability distribution obtained for the *full* system Eq. (1) are shown in Fig. 8. The latter corroborates that indeed no switching can be observed for the given parameter set in case of the homogeneous network. Nevertheless, for the sufficiently large g (small δ), the clustered network exhibits strong switching dynamics for the same (I, α) values, see the results for the *full* system Eq. (1) in Fig. 9. In Fig. 9(a), the sequences from the mean-rate dynamics of individual clusters $R_i(t)$ and the network rate $R_N(t)$ are shown, whereas in panel (b), the corresponding probability distributions are provided. Note that the network parameters are selected from the domain supporting maximal multistability, i.e., the region where the mean-field model (15) admits 9 different solutions, allowing for the coexistence of two inhomogeneous states within the same $\Sigma_l \otimes \Sigma_{m-l}$ symmetry subgroup.

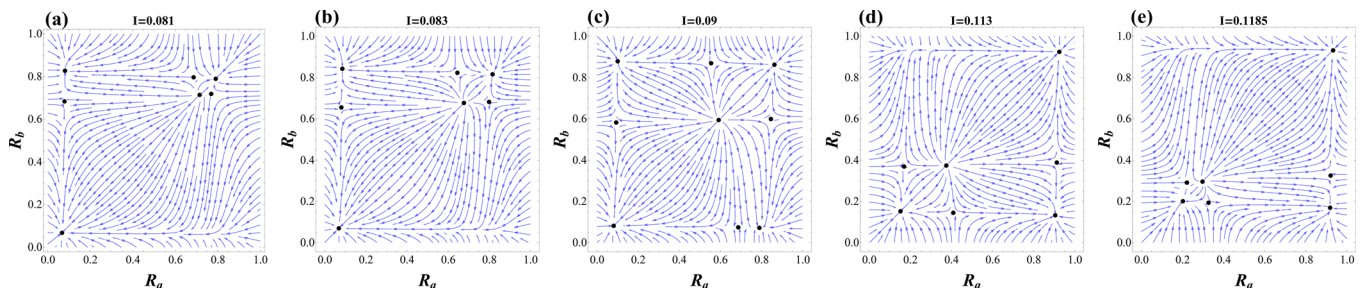


FIG. 7. Vector field plots indicating basins of attraction for the different types solutions of the mean-field model (15) in the (R_a, R_b) plane. The bias current I increases systematically from (a)-(e). The plots correspond to the example indicated in Fig. 5(b). The network parameters are $m = 5, B = 0.004, \delta = 0.004, \alpha = 0.8$.

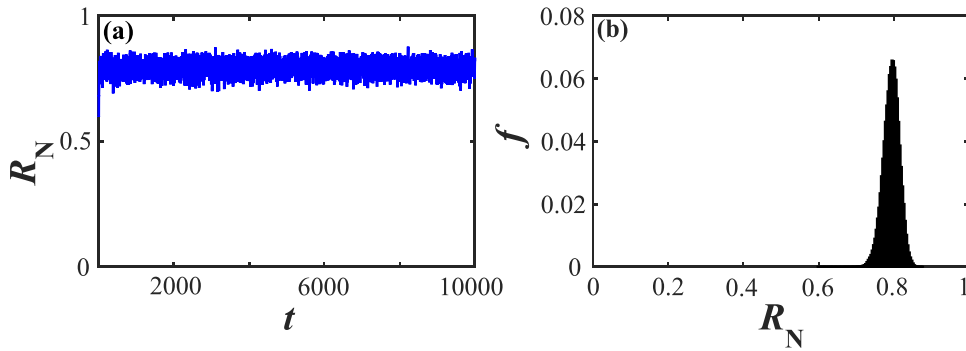


FIG. 8. Absence of switching dynamics for the *non-clustered* network beyond the vicinity of pitchfork bifurcation. In (a), the time trace of the network mean-rate $R_N(t)$ for the full system (1) is shown, whereas in (b), the corresponding stationary probability distribution $f(R)$ is provided. The network parameters are $\alpha = 0.9$, $I = 0.05$, $B = 0.01$, $N = 500$. Note that the selected (α, I) values lie within the $B = 0.01$ bistability tongue, but far from the cusp point, cf. Fig. 1(c).

The results in Figs. 8 and 9 indicate a good qualitative agreement between the dynamics of the full system and the effective model, in a sense that the analysis of the mean-field model can anticipate the parameter values where one may observe the switching dynamics in the full system. Naturally, the levels of the effective model obtained for the clustered network correspond to metastable states of the full system, whereby switching between them occurs due to the finite-size effects.

IV. CONCLUSION

In this paper, we have analyzed the interplay of clustered topology and different types of noise on the spontaneous activity of networks of rate-based neurons. Clustered topology appears to be biologically relevant,^{4,25,49} as the recent research on the microstructure of cortical networks has indicated that the small clusters of excitatory neurons are significantly over-represented.^{36,47} In real neural networks, the clusters may be important as functional units performing certain tasks⁴⁸ or may constitute processing units adapted to receiving a certain type of stimuli.^{50–52} We have demonstrated that clustering affects the collective dynamics of neural networks in a nontrivial fashion by promoting multistability such that spontaneous slow rate fluctuations gain on robustness.

From the theoretical perspective, our main contribution consists in derivation of the reduced system which describes the network activity in terms of interacting mean-field models representing each of the clusters. Typically, the reduced models address the two limit cases of a globally connected network^{32–34} or a network with the random sparse connectivity,^{30,35} such that the fluctuations of input between the units are small. The model presented here interpolates between these two scenarios, as the intra-cluster connectivity is strong, whereas the inter-cluster connectivity is weaker. We have identified three types of finite-size effects, including the small deterministic correction term, the macroscopic noise, and the topological uncertainty derived from the fact that each particular network realization features distinct deviations from the average connectivity degree. The macroscopic noise is a multiplicative one and incorporates three different sources of randomness, describing the impact of local neuronal noise on collective activity and the fluctuations in the input received by each of the units. Interestingly, the local intrinsic noise translates to additive macroscopic noise, whereas the microscopic external noise is reflected as multiplicative noise at the macroscopic level.

It has been demonstrated that the mean-field model can be used to qualitatively analyze the spontaneous activity of

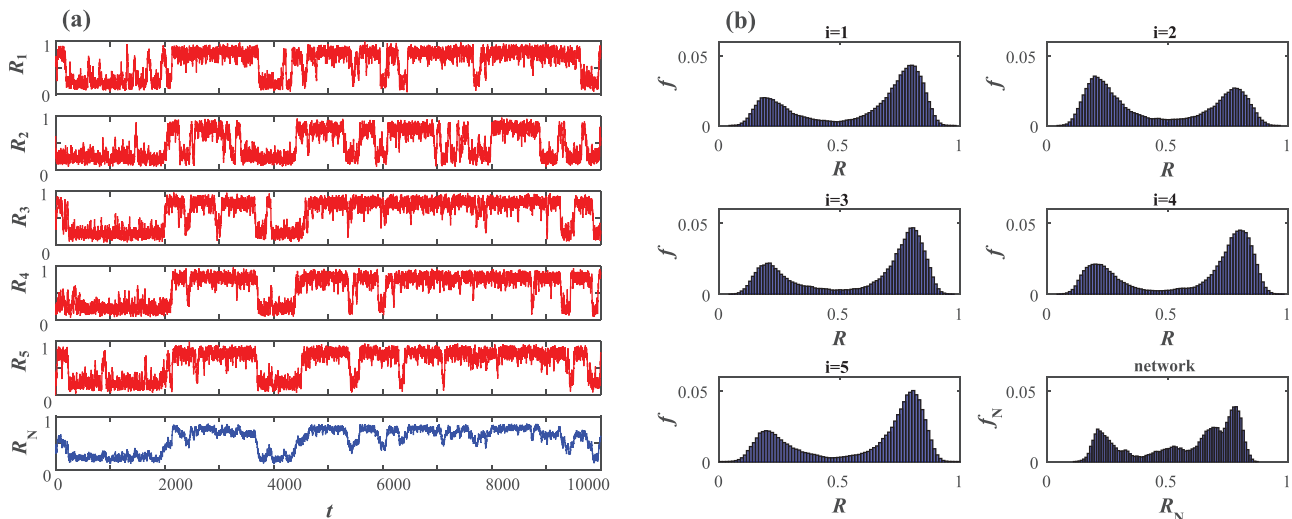


FIG. 9. Example of switching dynamics in the clustered network. Panel (a) shows the time traces of mean-rates of individual clusters $R_i(t)$, $i \in \{1, \dots, 5\}$ and the network $R_N(t)$ obtained by simulating the full system (1). In panel (b), the corresponding probability distributions $f(R)$ for the single clusters and the network are presented. The network parameters are $m = 5$, $B = 0.01$, $\alpha = 0.9$, $I = 0.0513$, $\delta = 0.01$, $N = 500$. The fact that clustering promotes multistability allows for the switching dynamics to occur in the much broader (I, α) domain than for the homogeneous random network, cf. Fig. 1(c) and the time series in Fig. 8.

the clustered network. The mechanism behind slow rate fluctuations has been explained by considering the stability and bifurcations of the mean-field model in the thermodynamic limit. The latter also allowed us to contrast the cases of the non-clustered and clustered network. In the non-clustered network, the crucial ingredient to slow rate fluctuations is that the network parameters lie close to pitchfork bifurcation. The evolution of the mean-rate may then locally be described by the paradigm of noise-driven motion of a particle in a double-well potential, so that its local minima coincide with the UP and DOWN states of the network. Such mechanism is *per se* generic, but lacks robustness, as it is confined to a small vicinity of the pitchfork bifurcation. The key effect of introducing clustering consists in the increased multistability of the network, facilitated by the onset and coexistence of states where different groups of clusters lie in the UP or the DOWN states. This promotes the switching dynamics, making it more efficient in a sense that alternation between the different network levels can be achieved just by changing the states of individual clusters rather than the whole network. Alternations within single clusters are naturally more likely since the finite-size effect associated to macroscopic noise is more pronounced. This way, the switching phenomenon gains on robustness, extending into the parameter domains where it cannot be observed for the non-clustered network.

The importance of clustered topology for macroscopic variability has earlier been indicated for the networks of spiking neurons with *balanced* excitatory-inhibitory input.^{4,24,25,53} However, with such local dynamics, slow fluctuations of the mean network activity cannot even be observed for a simple random network topology, which implies that clustering indeed plays the crucial role in inducing the switching behavior. Thus, our results on the rate-based neurons together with the previous work on spiking neurons suggest that promoting of slow rate fluctuations by clustered topology may indeed be a universal phenomenon independent on the particular model of local neuronal dynamics.

In view of the fact that the spontaneous activity of real neurons may indeed be described as a doubly stochastic process,^{54–56} combining the fluctuations on short and long timescales, the presented work has been aimed at providing theoretical tools for analysis of macroscopic variability in neural networks and its relation to microscopic dynamics and the network topology. We believe that the same method can be used to analyze the evoked activity of the network, examining the impact of clustering on the network's response to external stimulation. Also, our research so far has been confined to networks of excitatory neurons, but we believe that the same theoretical framework can readily be used to analyze the complex behavior of networks with both excitatory and inhibitory neurons. One expects that the presence of inhibitory subassembly should have a nontrivial impact both to spontaneous and evoked network activities.

ACKNOWLEDGMENTS

This work was supported by the Ministry of Education, Science and Technological Development of Republic of Serbia

under Project No. 171017 and by the Russian Foundation for Basic Research under Project No. 17-02-00904.

- ¹A. Destexhe, M. Rudolph, and D. Paré, *Nat. Rev. Neurosci.* **4**, 739 (2003).
- ²M. R. Cohen and A. Kohn, *Nat. Neurosci.* **14**, 811 (2011).
- ³B. B. Averbeck, P. E. Latham, and A. Pouget, *Nat. Rev. Neurosci.* **7**, 358 (2006).
- ⁴A. Litwin-Kumar and B. Doiron, *Nat. Neurosci.* **15**, 1498 (2012).
- ⁵M. Smith and A. Kohn, *J. Neurosci.* **28**, 12591 (2008).
- ⁶G. Buzsáki, C. A. Anastassiou, and C. Koch, *Nat. Rev. Neurosci.* **13**, 407 (2012).
- ⁷G. Buzsáki, *Rhythms of the Brain* (Oxford University Press, Oxford, 2006).
- ⁸T. T. G. Hahn, J. M. McFarland, S. Berberich, B. Sakmann, and M. R. Mehta, *Nat. Neurosci.* **15**, 1531 (2012).
- ⁹A. Destexhe, D. Contreras, and M. Steriade, *J. Neurosci.* **19**, 4595 (1999); available at <http://www.jneurosci.org/content/19/11/4595>.
- ¹⁰C. C. H. Petersen, T. T. G. Hahn, M. Mehta, A. Grinvald, and B. Sakmann, *Proc. Natl. Acad. Sci. U. S. A.* **100**, 13638 (2003).
- ¹¹V. V. Vyazovskiy and K. D. Harris, *Nat. Rev. Neurosci.* **14**, 443 (2013).
- ¹²T. T. G. Hahn, B. Sakmann, and M. R. Mehta, *Nat. Neurosci.* **9**, 1359 (2006).
- ¹³G. Gigante, G. Deco, S. Marom, and P. Del Giudice, *PLoS Comput. Biol.* **11**, e1004547 (2015).
- ¹⁴R. Cossart, D. Aronov, and R. Yuste, *Nature* **423**, 283 (2003).
- ¹⁵R. L. Cowan and C. J. Wilson, *J. Neurophysiol.* **71**, 17 (1994).
- ¹⁶D. Millman, S. Mihalas, A. Kirkwood, and E. Niebur, *Nat. Phys.* **6**, 801 (2010).
- ¹⁷M. Steriade, D. A. McCormick, and T. J. Sejnowski, *Science* **262**, 679 (1993).
- ¹⁸J. Anderson *et al.*, *Nat. Neurosci.* **3**, 617 (2000).
- ¹⁹D. Ji and M. A. Wilson, *Nat. Neurosci.* **10**, 100 (2007).
- ²⁰Y. Isomura *et al.*, *Neuron* **52**, 871 (2006).
- ²¹M. Remondes and E. M. Schuman, *Nature* **431**, 699 (2004).
- ²²S. Diekelmann and J. Born, *Nat. Rev. Neurosci.* **11**, 114 (2010).
- ²³D. Miyamoto, *et al.*, *Science* **352**, 1315 (2016).
- ²⁴F. Lagzi and S. Rotter, *PLoS ONE* **10**, e0138947 (2015).
- ²⁵B. Doiron and A. Litwin-Kumar, *Front. Comput. Neurosci.* **8**, 56 (2014).
- ²⁶M. D. McDonnell and L. M. Ward, *PLoS One* **9**, e88254 (2014).
- ²⁷M. D. McDonnell and L. M. Ward, *Nat. Rev. Neurosci.* **12**, 415 (2011).
- ²⁸A. A. Faisal, L. P. J. Selen, and D. M. Wolpert, *Nat. Rev. Neurosci.* **9**, 292 (2008).
- ²⁹R. Moreno-Bote, J. Rinzler, and N. Rubin, *J. Neurophys.* **98**, 1125 (2007).
- ³⁰I. Franović and V. Klinshov, *Europhys. Lett.* **116**, 48002 (2016).
- ³¹L. Albantakis and G. Deco, *PLoS Comput. Biol.* **7**, e1002086 (2011).
- ³²B. Lindner, J. Garcia-Ojalvo, A. Neiman, and L. Schimansky-Geier, *Phys. Rep.* **392**, 321 (2004).
- ³³M. A. Zaks, X. Sailer, L. Schimansky-Geier, and A. B. Neiman, *Chaos* **15**, 026117 (2005).
- ³⁴I. Franović, K. Todorović, N. Vasović, and N. Burić, *Phys. Rev. E* **87**, 012922 (2013).
- ³⁵V. Klinshov and I. Franović, *Phys. Rev. E* **92**, 062813 (2015).
- ³⁶R. Perin, T. K. Berger, and H. Markram, *Proc. Natl. Acad. Sci. U. S. A.* **108**, 5419 (2011).
- ³⁷L. Zemanová, C. Zhou, and J. Kurths, *Physica D* **224**, 202 (2006).
- ³⁸W. Gerstner, W. M. Kistler, R. Naud, and L. Paninski, *Neuronal Dynamics: From Single Neurons to Networks and Models of Cognition* (Cambridge University Press, Cambridge, 2014).
- ³⁹H. Hasegawa, *Phys. Rev. E* **75**, 051904 (2007).
- ⁴⁰R. A. Anderson, S. Musallam, and B. Pesaran, *Curr. Opin. Neurobiol.* **14**, 720 (2004).
- ⁴¹I. Franović, K. Todorović, N. Vasović, and N. Burić, *Phys. Rev. Lett.* **108**, 094101 (2012).
- ⁴²A. N. Burkitt, *Biol. Cybern.* **95**, 1 (2006).
- ⁴³V. I. Mel'nikov, *Phys. Rep.* **209**, 1 (1991).
- ⁴⁴C. W. Gardiner, *Handbook of Stochastic Methods for Physics, Chemistry and the Natural Sciences* (Springer-Verlag, Berlin, 2004).
- ⁴⁵A. Bovier and F. den Hollander, *Metastability, a Potential-Theoretic Approach* (Springer International Publishing, Switzerland, 2015).
- ⁴⁶G. A. Pavliotis, *Stochastic Processes and Applications* (Springer, New York, 2014).
- ⁴⁷S. Song, P. Sjöström, M. Reigl, S. Nelson, and D. Chklovskii, *PLoS Biol.* **3**, e68 (2005).

- ⁴⁸L. Yassin, B. L. Benedetti, J. Jouhanneau, J. A. Wen *et al.*, *Neuron* **68**, 1043 (2010).
- ⁴⁹E. L. Lameu, C. A. Batista, A. M. Batista, K. Iarosz, R. L. Viana, S. R. Lopes, and J. Kurths, *Chaos* **22**, 043149 (2012).
- ⁵⁰S. B. Hofer, H. Ko, B. Pichler, J. Vogelstein, H. Ros *et al.*, *Nat. Neurosci.* **14**, 1045 (2011).
- ⁵¹H. Ko, S. B. Hofer, B. Pichler, K. A. Buchanan, P. J. Sjöström, and T. D. Mrsic-Flogel, *Nature* **473**, 87 (2011).
- ⁵²Y. Yoshimura, J. L. M. Dantzker, and E. M. Callaway, *Nature* **433**, 868 (2005).
- ⁵³G. Deco and E. Hugues, *PLoS Comput. Biol.* **8**, e1002395 (2012).
- ⁵⁴M. Churchland and L. Abbott, *Nat. Neurosci.* **15**, 1472 (2012).
- ⁵⁵A. Ponce-Alvarez, A. Thiele, T. D. Albright, G. R. Stoner, and G. Deco, *Proc. Natl. Acad. Sci. U. S. A.* **110**, 13162 (2013).
- ⁵⁶B. M. Yu, J. P. Cunningham, G. Santhanam, S. I. Ryu, K. V. Shenoy, and M. Sahani, *J. Neurophysiol.* **102**, 614 (2009).